International Journal of Concrete Structures and Materials
Vol.11, No.2, pp.391–401, June 2017
DOI 10.1007/s40069-017-0200-0
ISSN 1976-0485 / eISSN 2234-1315

Mechanical Properties of Steam Cured High-Strength Steel Fiber-Reinforced Concrete with High-Volume Blast Furnace Slag

Jun-Mo Yang[1)], Doo-Yeol Yoo[2)], You-Chan Kim[3)], and Young-Soo Yoon[3),*]

(Received December 2, 2016, Accepted March 29, 2017, Published online May 19, 2017)

Abstract: In this study, the effects of water-to-binder (W/B) ratio and replacement ratio of blast furnace slag (BFS) on the compressive strength of concrete were first investigated to determine an optimized mixture. Then, using the optimized high-strength concrete (HSC) mixture, hooked steel fibers with various aspect ratios and volume fractions were used as additives and the resulting mechanical properties under compression and flexure were evaluated. Test results indicated that replacement ratios of BFS from 50 to 60% were optimal in maximizing the compressive strength of steam-cured HSCs with various W/B ratios. The use of hooked steel fibers with the aspect ratio of 80 led to better mechanical performance under both compression and flexure than those with the aspect ratio of 65. By increasing the fiber aspect ratio from 65 to 80, the hooked steel fiber volume content could be reduced by 0.25% without any significant deterioration of energy absorption capacity. Lastly, complete material models of steel-fiber-reinforced HSCs were proposed for structural design from Lee's model and the RILEM TC 162-TDF recommendations.

Keywords: high-strength concrete, blast furnace slag, hooked steel fiber, aspect ratio, mechanical property, material model.

1. Introduction

In recent years, the development of green concrete with low CO_2 emissions has received a great deal of attention from researchers worldwide (Bilodeau and Malhotra 2000; Menéndez et al. 2003; Mahmoud et al. 2013; Kinoshita et al. 2014). The production of Portland cement contributes a large portion of anthropogenic CO_2 emissions; thus, a key challenge is to reduce the amount of cement used in concrete mixtures. Replacing Portland cement with mineral admixtures such as fly ash, blast furnace slag (BFS), and silica fume has been a widely adopted strategy due to their pozzolanic reactivity and latent hydraulic activity (Jeon et al. 2006; Roychand et al. 2016). In particular, if the size of mineral particles is properly determined, then they can be used to fabricate concrete mixtures stronger than those without mineral admixtures. High-strength concrete (HSC) has many advantages for use in precast pre- or post-tensioned structures, which are normally steam-cured with heat. Thus, optimized mixtures need to be developed for steam-cured HSCs incorporating high volumes of mineral admixtures.

HSC is intrinsically brittle, exhibiting low fracture energy. This has limited the practical applications of HSC in real civil and architectural structures, and is especially limiting for designs subjected to tension or flexure. Several methods have been used to improve the ductility and energy absorption capacity of concrete, such as adding discontinuous fibers (i.e. steel, polymeric, and carbon fibers) and strengthening with fiber-reinforced polymers (Banthia and Nandakumar 2006; Myers et al. 2008; Kwon et al. 2015; Yoo and Yoon 2016d). The use of discontinuous fibers has been the most widely adopted method because it is the simplest and most effective in improving the ductility of concrete. According to a previous study performed by Bindiganavile and Banthia (2001), the use of steel fibers improved static post-cracking flexural behavior relative to polymeric fibers, especially at small deflections, because the polymeric fibers allowed wider cracks to form that carry tensile stress further beyond the matrix cracking. Yao et al. (2003) also reported much better flexural performance in concretes using steel fibers compared to those using polymeric fibers. Soroushian and Bayasi (1991) experimentally investigated the effect of steel fiber shape on the mechanical properties of concrete, and found that the use of hooked steel fibers having various aspect ratios was more effective in improving the flexural strength, energy absorption capacity, and post-peak ductility under compression than the use of straight and crimped fibers at identical volume fractions of 2%. Thus, among the various types of steel and polymeric fibers available, synthetically hooked steel fibers are

[1)]Steel Structure Research Group, POSCO, 100, Songdogwahak-ro, Yeonsu-gu, Incheon 21985, South Korea.

[2)]Department of Architectural Engineering, Hanyang University, 222 Wangsimni-ro, Seongdong-gu, Seoul 04763, South Korea.

[3)]School of Civil, Environmental and Architectural Engineering, Korea University, 145 Anam-ro, Seongbuk-gu, Seoul 02841, South Korea.

*Corresponding Author; E-mail: ysyoon@korea.ac.kr

expected to be most efficient in improving the flexural performance of concrete under static loads assuming identical amount of added fibers.

To allow the practical use of such fiber-reinforced concrete (FRC) in actual structures, its material models need to be preferentially proposed. Fibers incorporated into the cement matrix inhibit crack propagation and widening, leading to different post-cracking behaviors under compression and tension compared to those of ordinary concrete without fiber. For this reason, several researchers (Barros et al. 2005) have previously used RILEM TC 162-TDF recommendations (RILEM 2000), one of the most widely used model codes for FRC compositions including metallic fibers. However, RILEM TC 162-TDF recommends the use of a compressive model of FRC that is identical to that used for ordinary concrete, even though FRC's post-peak ductility is substantially influenced by the fibers (Yoo et al. 2015). Thus, it is reasonable to develop a model of tensile stress and strain (TSS) based on RILEM TC 162-TDF and to develop a better model of compressive stress and strain (CSS) based instead upon previously suggested compressive models for FRC.

Accordingly, in the present study, the effects of water-to-binder (W/B) ratio and BFS replacement ratio upon concrete compressive strength were first examined to determine optimized mix proportions. Then, the mechanical properties of the optimized HSC were investigated for various aspect ratios and volume fractions of hooked steel fiber additive. Based upon our work, herein we propose complete material models of steel-fiber-reinforced HSC (SFR-HSC) based on previous models and the RILEM TC 162-TDF recommendations.

2. Test Program

2.1 Materials, Mixture Proportions, and Curing Condition

Table 1 details the mixture proportions tested. To obtain optimized mixture proportions in terms of maximizing early age compressive strength, three different W/B ratios of 25, 27.5, and 30% and five different ratios of cement replacement by BFS (0, 40, 50, 60, and 70%) were tested. The unit water content was held constant at 163 kg/m^3, and various fine aggregate ratios (s/a) from 41 to 44% were used. Type I Portland cement and Type III BFS were adopted as cementitious materials; Tables 2 and 3 respectively list their chemical compositions and physical properties. Type III BFS was chosen from the economical point of view. Crushed aggregate was adopted as the fine aggregate, and coarse aggregate of maximum size 20 mm was also used. A polycarboxylic acid based air-entraining and water-reducing admixture was incorporated to attain the required workability. The workability of concrete without fibers and with fibers was controlled by 600 and 450 mm slump flow, respectively.

To improve the ductility of the optimized low-carbon HSC mixture containing BFS, hooked steel fibers with two different aspect ratios were considered: $l_f/d_f = 35/0.55 = 65$ and $l_f/d_f = 60/0.75 = 80$, where l_f is the fiber length and d_f is the fiber diameter. Table 4 summarizes the physical and geometrical properties of the steel fibers used. The volume fractions of steel fibers used were 0.5 and 0.75%. For the optimized mixtures including hooked steel fibers, various mechanical properties were investigated including compressive strength, elastic modulus, and flexural performance, and complete material models for structural design are suggested herein based on previous work and the RILEM TC 162-TDF recommendations.

Steam curing with heat was adopted in this study, because the low-carbon SFR-HSC developed herein is intended for precast prestressed concrete products. For the first 4 h, all of the specimens were cured at approximately 20 °C with a relative humidity (RH) of 60%; thereafter, the curing temperature was increased from 20 to 60 °C for 2 h with steam, and then these conditions were maintained for 6 h. Then, the temperature was decreased to 20 °C using a 3 h ramp, and the conditions were maintained at 20 °C and 60% RH until the testing date (Fig. 1).

2.2 Test Setup and Specimen Preparation

2.2.1 Compression

Five cylindrical specimens for each variable were used in the compressive strength tests. Specimens were of diameter 100 mm and height 200 mm. Before testing, all cylinders were ground with a diamond blade to eliminate any eccentricities. To measure elastic moduli, each specimen was fitted with a compressometer equipped with three linear variable differential transformers (LVDTs). A uniaxial load was applied at the monotonic rate of 0.1 mm/min using a universal testing machine with the maximum capacity of 250 ton. The compressive tests were carried out according to ASTM C39 (ASTM 2014); the test setup is shown in Fig. 2.

2.2.2 Four-Point Flexure

Three concrete prisms of cross-section 100 × 100 mm^2 and length 400 mm were used for each variable in tests of flexural properties. To minimize the effects of eccentricities, all specimens were rotated 90° from their casting surface before testing. A uniaxial load was applied at the rate of 0.4 mm/min using the same universal testing machine used for compressive testing. To measure the pure mid-span deflection without support settlement, a yoke equipped with one LVDT on each side was installed. A pin-type support was adopted to maintain the clear span length of 300 mm, to aid in calculating the flexural strength, and the applied load was measured using a load cell affixed to the cross head. The flexural strength was calculated using the equation PL/bh^2, where P is the applied load, L is the clear span length, b is the beam width, and h is the beam height. The test setup used for four-point flexural testing is illustrated in detail in Fig. 3.

2.2.3 Three-Point Flexure for Notched Beams

To properly design FRC structures subject to flexure or tension, a TSS model needs to be proposed for sectional analysis (Yoo et al. 2016a). For this, RILEM TC 162-TDF

Table 1 Mixture proportions.

W/B (%)	BFS/B (%)	s/a (%)	Unit weight (kg/m^3)					
			Water	Cement	BFS	Fine aggregate	Coarse aggregate	AEWR agent
25.0	0	43.7	163	652	0	682	882	0.80
	40	42.0		391	261	647	897	0.65
	50	41.7		326	326	641	899	0.70
	60	41.4		261	391	634	901	0.75
	70	41.1		196	456	628	903	0.70
27.5	0	43.7		593	0	703	909	0.77
	40	43.0		356	237	685	911	0.60
	50	42.7		296	296	678	913	0.63
	60	42.4		237	356	671	916	0.70
	70	42.1		178	415	665	918	0.68
30.0	0	43.7		543	0	721	932	0.80
	40	44.0		326	217	719	919	0.63
	50	43.7		272	272	712	921	0.60
	60	43.4		217	326	706	924	0.68
	70	43.1		163	380	699	927	0.70

W/B water-to-binder ratio, *BFS/B* ratio between blast furnace slag and total binder (cement + blast furnace slag), *s/a* ratio between amount of fine aggregate and total amount of aggregate, *BFS* blast furnace slag, and *AEWR agent* air-entraining and water-reducing agent.

Table 2 Chemical compositions and physical properties of Type I Portland cement.

Surface area (cm^2/g)	Density (g/cm^3)	Ig.loss (%)	Chemical composition (%)					
			SiO_2	Al_2O_3	Fe_2O_3	CaO	MgO	SO_3
3413	3.15	1.40	21.25	5.28	3.02	61.00	3.71	1.24

Table 3 Chemical compositions and physical properties of Type III blast furnace slag.

Surface area (cm^2/g)	Density (g/cm^3)	Ig.loss (%)	Chemical composition (%)		
			SiO_2	MgO	Cl^-
4250	2.90	0.32	21.01	6.40	0.005

Table 4 Properties of hooked steel fibers.

Name	Diameter, d_f (mm)	Length, l_f (mm)	Aspect ratio (l_f/d_f)	Density (g/cm^3)	Tensile strength (MPa)	Elastic modulus (GPa)
Short HS	0.55	35	65	7.9	1400	200
Long HS	0.75	60	80	7.9	1100	200

HS hooked steel fiber.

proposes a method based on a simple three-point flexural test. According to the RILEM recommendations, beams of dimensions 150 × 150 × 550 mm^3 were fabricated, and three specimens were tested for each variable. For three-point-flexure tests, a uniaxial load was monotonically applied at the rate of 0.4 mm/min using the universal testing machine, conditions identical to those used for the compressive and four-point flexural tests. A 25 mm notch was cut into the beam at the middle of its length to induce the propagation of a single crack, and a yoke with two LVDTs was also installed to measure the pure mid-span deflection. During the three-point flexural tests, a roller-type support was used to eliminate friction between the beam and the support, as shown in Fig. 4.

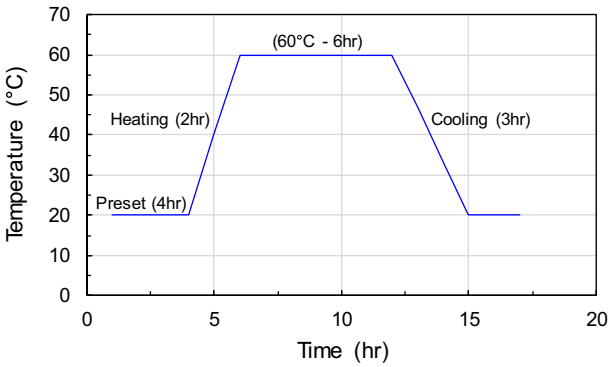

Fig. 1 Temperature history for steam curing.

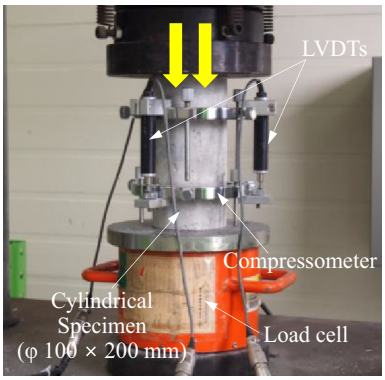

Fig. 2 Compressive test (ASTM C39).

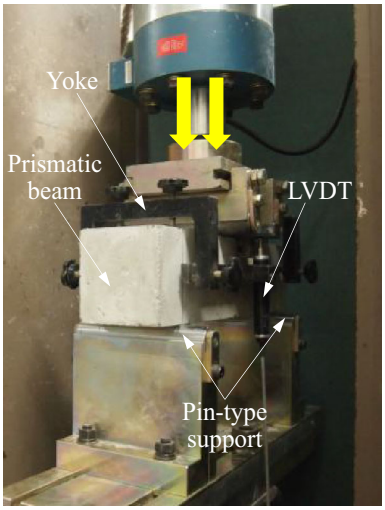

Fig. 3 Four-point flexural test (ASTM C1609).

3. Test Results and Discussion

3.1 Effects of W/B and Replacement Ratio of BFS on Compressive Strength

Compressive strengths were tested and the results are given in Fig. 5. In the figure and hereinafter, the letters OPC and BS indicate concrete specimens respectively incorporating ordinary Portland cement without BFS and incorporating both OPC and BFS; numbers subsequent to the BS designation denote the percentage of the BFS replacement ratio. For example, BS60 indicates concrete with the BFS replacement ratio of 60%. The compressive strength generally increased with increasing curing age, because of the continuous generation of calcium-silicate-hydrate (C-S-H) owing to cement hydration and pore filling. Normally, concrete containing both OPC and BS has a higher compressive strength than concrete made with OPC only. Concrete containing BS has a higher proportion of the strength-enhancing C-S-H than concrete made with OPC only. In addition, cylinders prepared using lower W/B ratios exhibited slightly higher compressive strengths than their higher-W/B counterparts with equivalent holding age and BFS replacement ratios. It is well known that lower W/B ratios yield higher compressive strengths, owing to their formation of dense, low-porosity microstructures. Regardless of the W/B ratio, cylinders including BFS with replacement ratios of up to 60% provided greater compressive strength than those with OPC only. Interestingly, higher early-age compressive strengths were also observed for mixtures including BFS, compared to those without BFS. This finding conflicted with previous reports (Mindess et al. 2003) that, because of the latent hydraulic activity of BFS, concrete with BFS normally exhibits lower strength at early ages, but higher strength during long-term aging than concrete without BFS. The main reason why specimens including BFS showed higher strengths in the present work, even at early ages, is that the proportion of C-S-H and the apparent activation energy of concrete increased with increasing BFS replacement ratio, regardless of the W/B ratio. According to a previous study performed by Barnett et al. (2006), under standard curing conditions, mortar including BFS exhibited slower strength development than that of mortar composed of Portland cement only, whereas under higher curing temperatures, the strength gain was much faster and the enhancement of early-age strength was more significant for cements with higher BFS replacement ratios, apparently owing to the greater activation energy. Thus, it can be concluded that replacing cement with BFS (at $\leq$60%) leads to improvement in compressive strength, both early and long-term aging.

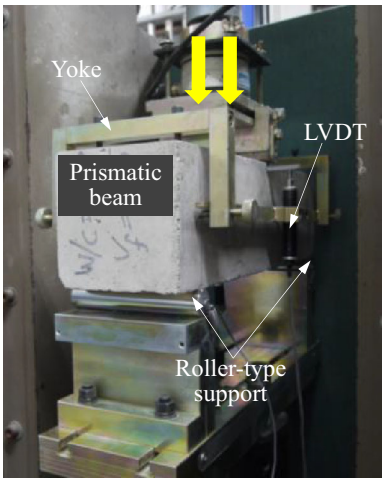

Fig. 4 Three-point flexural test for notched beam (RILEM TC 162-TDF).

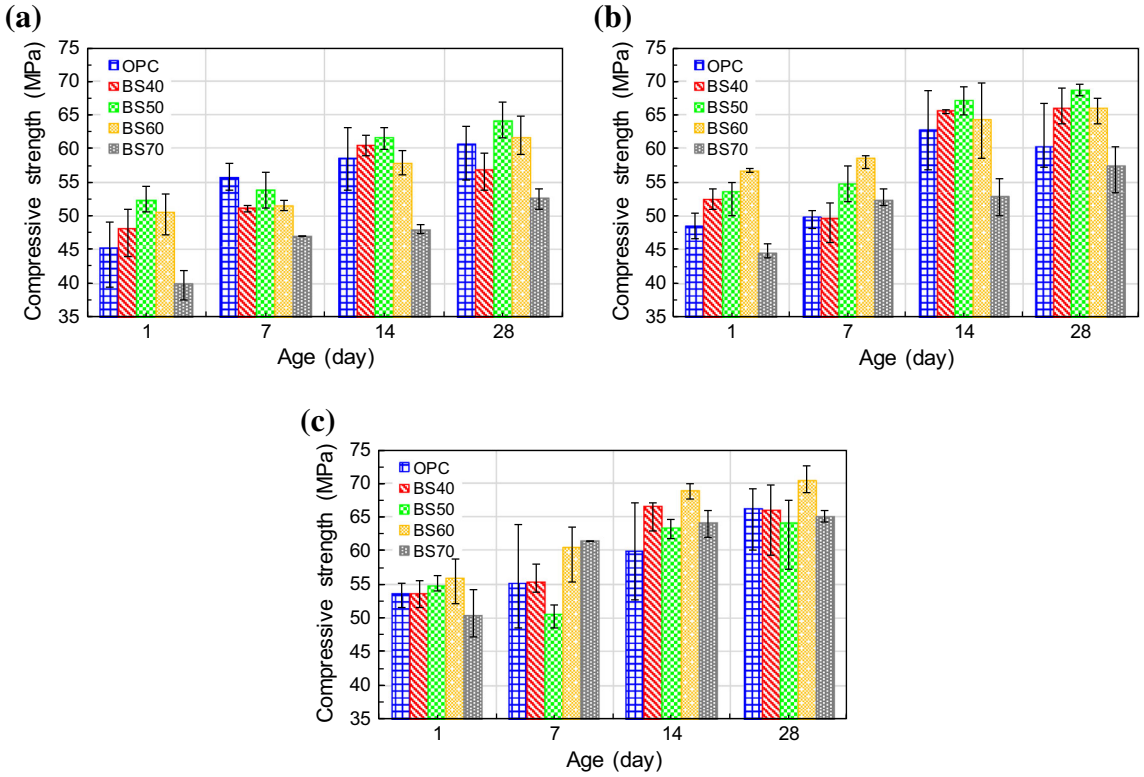

Fig. 5 Summary of compressive strength; **a** W/B of 0.3, **b** W/B of 0.275, **c** W/B of 0.25.

Figure 6 shows the compressive strengths at various curing ages for concretes with various BFS replacement ratios. In the case of 0.3 W/B, BS50 exhibited the highest compressive strengths regardless of the curing age. In the case of 0.25 W/B, BS60 showed the highest compressive strengths. In the case of 0.275 W/B, BS60 showed the highest compressive strength early (before 7 d), whereas BS50 showed the highest strength later (after 14 d). Overall, it was noted that the BFS replacement ratios of 50–60% were most effective in improving the compressive strength of steam-cured HSC, both early and long-term aging.

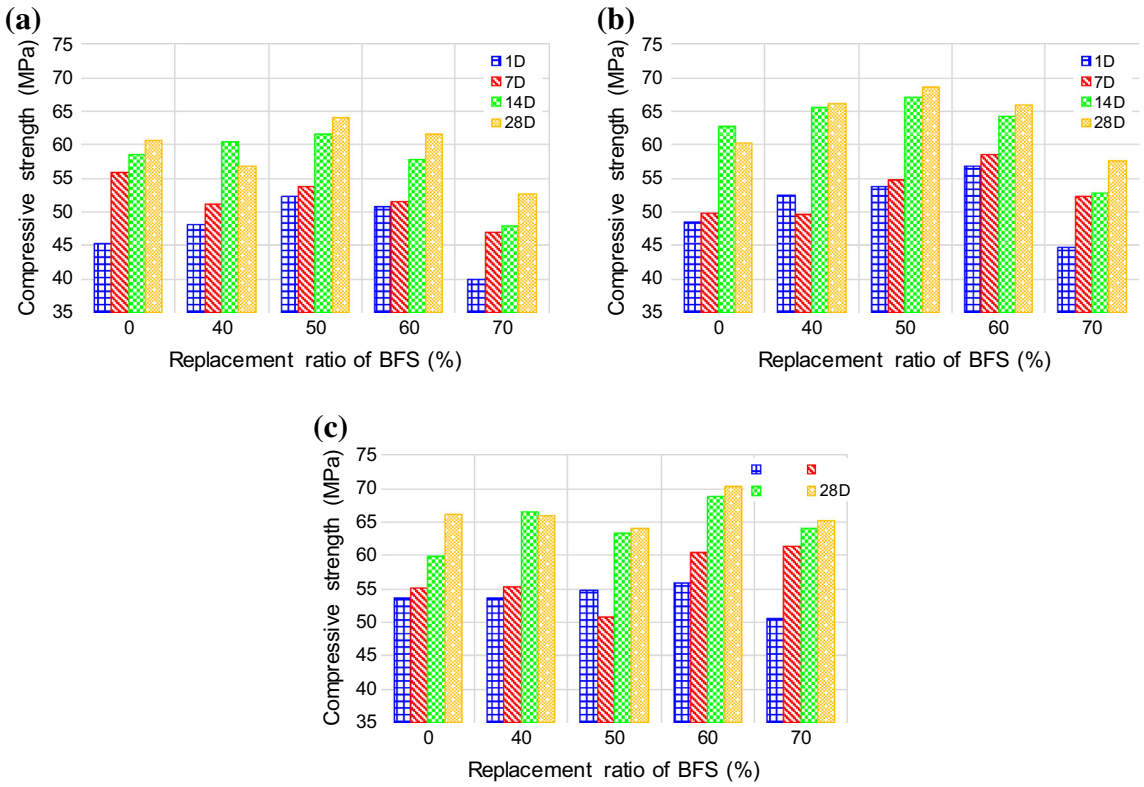

Fig. 6 Effect of replacement ratio of BFS on compressive strength; **a** W/B of 0.3, **b** W/B of 0.275, **c** W/B of 0.25.

The chief aim of the present study was to develop low-carbon HSC mixtures for precast prestressed products; thus the initial strength immediately after heat curing was the most important parameter. The highest 1-d compressive strength of 56.7 MPa was obtained from mixture BS60 at the W/B of 0.275. In addition, when a W/B ratio of 0.25 was used, the workability was obviously deteriorated and slightly higher AE agent was required, as compared with W/B ratio of 0.275 or 0.3. Thus, this mixture was considered optimal for precast prestressed concrete products in this study.

3.2 Properties of SFR-HSC

ACI Subcommittee 318-F recommended the use of a minimum fiber volume fraction (V_f) of 0.75% for replacing minimum shear reinforcement through the use of steel fibers (Parra-Montesinos 2006). Thus, we first used the V_f of 0.75 vol. % of hooked steel fibers having the aspect ratio of 65. According to previous studies (Yazıcı et al. 2007; Yoo and Yoon 2015; Yoo et al. 2016b), the use of steel fibers having higher aspect ratios exhibited better flexural performance than those having lower aspect ratios. Thus, to investigate whether the content of hooked steel fibers could be reduced by increasing the aspect ratio, concrete beams including 0.5 vol.% of hooked steel fibers with the higher aspect ratio of 80 were also prepared and tested. Also, to fundamentally evaluate how much the flexural performance of HSC beams could be improved by increasing the fiber aspect ratio, a specimen containing 0.5 vol.% of hooked steel fibers having the smaller aspect ratio of 65 was also prepared and tested. The optimized mixture (BS60 with W/B of 0.275) was used, and thus the designation system adopted herein for such samples only specifies the fiber aspect ratio and volume fraction, as follows: aspect ratio of steel fiber (Sxx)-volume fraction (0. yy). Herein, xx and yy respectively represent the aspect ratio and volume fraction. For example, S65-0.75 indicates the specimen including 0.75 vol.% of steel fibers each having the aspect ratio of 65.

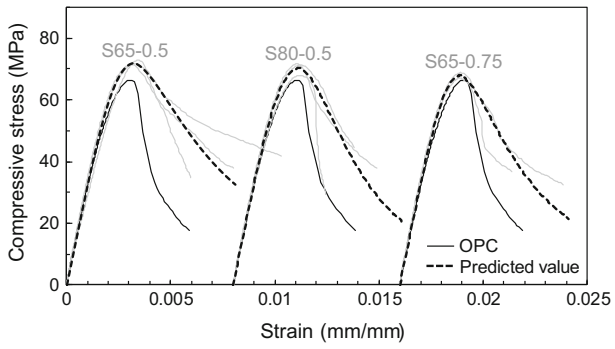

Fig. 7 Average compressive stress versus strain curves (after 28 days).

3.2.1 Compressive Behaviors

Compressive stress–strain curves for all test cylinders were acquired after 28 d and are shown in Fig. 7. To indicate the effect of including the hooked steel fibers, all figures include the average compressive stress–strain curve of the concrete mixture without fiber, designated OPC. Samples including hooked steel fibers had slightly greater compressive strength and substantially improved post-peak ductility. This is consistent with findings by Ezeldin and Balaguru (1992), and arises from the steel fibers' inhibition of crack propagation and opening.

Table 5 summarizes compressive strength, strain capacity, and elastic modulus measurements. The specimens including steel fibers of aspect ratio 65 (S65-0.5 and S65-0.75) exhibited higher compressive strength, strain capacity, and elastic modulus compared to that without fiber. Specimen S80-0.5 exhibited higher strength and elastic modulus but lower strain capacity than that without fiber. The ascending stress–strain curve of this specimen was more linear than that of its counterpart without fiber, because of its inhibition of micro-crack propagation, but the improvement of compressive strength was relatively small. In addition, the micro-crack control performance of specimen S80 was worse than that of specimens S65 because the steel fibers included in specimen S80 have larger diameter and length than the fibers included in specimens S65. The smaller fibers can cross cracks more easily under the condition of same fiber volume percentage. Thus, it can be noted that the use of hooked steel fibers with smaller aspect ratios is more effective in improving the compressive performance of HSC.

To predict the compressive behaviors of SFR-HSC, the following equation suggested by Lee et al. (2015) was adopted.

$$f_c = f_c' \left[\frac{\alpha\left(\frac{\varepsilon}{\varepsilon_0}\right)}{\alpha - 1 + \left(\frac{\varepsilon}{\varepsilon_0}\right)^{\beta}} \right] \tag{1}$$

Herein,

$$\alpha = \beta = \frac{1}{1 - \left(\frac{f_c'}{\varepsilon_0 E_c}\right)} \quad \text{for } \frac{\varepsilon}{\varepsilon_0} \leq 1.0$$

Table 5 Summary of compressive properties (at 28 days).

Name	Compressive strength (MPa)	Strain capacity (mm/mm)	Elastic modulus (GPa)
OPC	67.0	0.00310	32.0
S65-0.5	70.3	0.00320	33.0
S80-0.5	72.0	0.00326	32.9
S65-0.75	67.9	0.00292	33.0

$$\alpha = 1 + 0.723\left(V_f \frac{l_f}{d_f}\right) \quad \text{for } \frac{\varepsilon}{\varepsilon_0} > 1.0$$

$$\beta = \left(\frac{f_c'}{50}\right)^{0.064}\left[1 + 0.882\left(V_f \frac{l_f}{d_f}\right)^{-0.882}\right] \geq \alpha \quad \text{for } \frac{\varepsilon}{\varepsilon_0} > 1.0$$

where f_c' is the compressive strength, ε_0 is the strain capacity, α and β are coefficients, E_c is the elastic modulus, V_f is the fiber volume fraction of fiber, l_f is the fiber length, and d_f is the fiber diameter.

In Fig. 7, the dotted line indicates the values predicted by Eq. (1). An empirical equation proposed by Lee et al. (2015) appeared to be appropriate for predicting the compressive behavior of SFR-HSC with high-volume BFS, for both ascending and descending branches.

3.2.2 Flexural Behaviors

Curves of flexural load versus deflection are shown in Fig. 8, and Table 6 summarizes several important parameters describing the flexural behavior. The flexural strengths of concrete beams under four-point flexure were calculated using the equation $f = PL/bh^2$, where P is the applied load, L is the clear span length, b is the beam width, and h is the beam height. The specimen without fiber (OPC) exhibited a sudden load drop immediately after its first cracking. In contrast, the specimens with fibers sustained the flexural load well even after the first crack formation, due to fiber bridging. The specimens including steel fibers (S65-0.5, S65-0.75, and S80-0.5) showed deflection-hardening behavior, leading to higher load carrying capacity even after the first cracking, whereas the OPC specimen demonstrated deflection-softening behavior. This is supported by the measured values of deflection capacity (i.e., the deflection corresponding to the point of flexural strength) given in Table 6. The deflection capacities of specimens with steel fibers were much higher than that of the specimen without fiber. In addition, specimen S80-0.5 demonstrated the flexural strength of 9.8 MPa, quite similar to that of S65-0.75 ($f_{MOR} = 10.0$ MPa; f_{MOR} is the post-cracking flexural strength) and higher than that of S65-0.5 ($f_{MOR} = 8.0$ MPa).

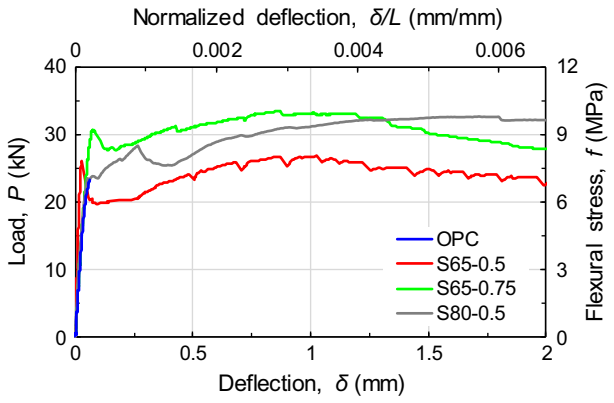

Fig. 8 Flexural load versus deflection curves (four-point flexure).

In addition, specimen S80-0.5 exhibited the largest deflection capacity of 1.72 mm, owing to its greater length. From these observation, it can be concluded that the use of hooked steel fibers with higher aspect ratios is more effective in improving the flexural strength and deflection capacity.

The toughness values at two deflection points of $L/600$ and $L/150$ were calculated according to ASTM C1609 (ASTM 2012); L is the clear span length. Because the specimen without fibers exhibited a sudden load drop immediately after the first cracking (at 0.063 mm deflection), its toughness was not calculated. Specimen S65-0.75 exhibited the highest toughnesses at both deflection points because it had the largest amount of steel fibers among the specimens studied. However, specimen S80-0.5 demonstrated toughness values quite similar to those of S65-0.75 despite its lower amount of fibers, and showed higher toughness values than S65-0.5. This indicates that the use of steel fibers with higher aspect ratios can reduce the amount of fibers needed without any noticeable reduction of energy absorption capacity, a finding consistent with previous findings mentioned above regarding flexural strength and deflection capacity.

ACI 318-14 code (ACI 2014) indicates that concrete with steel fibers can be used for shear resistance provided that the residual strengths, f_R, obtained from four-point flexural tests (ASTM C1609) at the deflection points of $L/300$ and $L/150$ are greater than 90 and 75% of the f_{LOP}. Therefore, the residual flexural stress was also investigated; Table 6 summarizes the results. All test series satisfied the requirements of the ACI 318 code. This means that SFRC containing 0.5 vol. % of hooked steel fibers having aspect ratios higher than 65 are suitable to be used to impart shear resistance. Interestingly, the residual flexural strengths were increased more significantly with increasing fiber aspect ratio than with a small increase in the amount of steel fibers. Thus, it was concluded that using steel fibers with higher aspect ratios is effective in increasing residual strength, affecting shear resistance, than using those with smaller ones.

3.2.3 Suggestion of Tensile Stress Block for Structural Design

Curves of flexural load versus deflection of large-sized beams under three-point flexure are shown in Fig. 9. Similar to the results obtained in four-point flexure testing, specimens including steel fibers exhibited better post-cracking flexural behavior than that without fiber, and specimen S80-0.5 exhibited similar flexural strength and higher deflection capacity than specimen S65-0.75, even though its fiber content was lower. Herein, the flexural strength of three-point bending was calculated by using the equation $f = 3PL/2b(h - a_0)^2$, where a_0 is the notch depth.

The flexural strengths at the points of LOP and MOR obtained in the larger beams were clearly lower than those obtained in the smaller beams (in Fig. 8). This was mainly caused by the size effect and restraint of the support. Decreases in the strength of normal- and high-strength SFRC beams has been previously reported by Yoo et al. (2016c). In accordance with Weibull's size effect theory (Weibull 1939),

Table 6 Parameters obtained from four-point flexural tests (ASTM C1609).

Name	F_{LOP} (MPa)	F_{MOR} (MPa)	δ_{MOR} (mm)	Tough$_{L/600}$ (kNmm)	Tough$_{L/150}$ (kNmm)	$F_{R,L/300}$ (MPa)	$F_{R,L/150}$ (MPa)
OPC	7.0	7.0	0.063	–	–	–	–
S65-0.5	7.8	8.0	0.85	10.8	48.4	8.0 (103%)	6.8 (87%)
S80-0.5	7.2	9.8	1.72	12.5	59.8	9.4 (131%)	9.6 (133%)
S65-0.75	9.2	10.0	0.87	14.1	60.9	9.9 (108%)	8.3 (90%)

f_{LOP} first cracking flexural strength, f_{MOR} post-cracking flexural strength, δ_{MOR} deflection capacity, Tough$_{L/600}$ toughness at $L/600$, Tough$_{L/150}$ toughness at $L/150$, $f_{R,L/300}$ residual flexural stress at $L/300$, $f_{R,L/150}$ residual flexural stress at $L/150$.

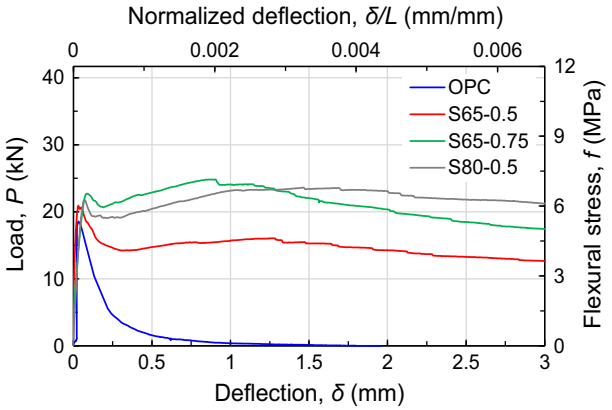

Fig. 9 Flexural load versus deflection curves (three-point flexure).

larger specimens are normally weaker than smaller ones because they have a greater chance to include larger and more severe flaws. The three-point flexural tests were performed using a roller-type support to eliminate the support restraint as per RILEM TC 162-TDF, whereas the four-point flexural tests were carried out using a pin-type support as per ASTM C1609. In test results reported by Wille and Parra-Montesinos, the measured flexural strength was clearly affected by the support conditions: use of the pin-type support resulted in a higher flexural strength than the roller-type support due to its restraint by friction (Wille and Parra-Montesinos 2012).

To calculate a tensile stress block, RILEM TC 162-TDF recommendations were adopted in this study. Firstly, equivalent flexural strengths were calculated based on energy absorption capacities, as follows:

$$f_{eq,2} = \frac{3}{2}\frac{D^f_{BZ,2}}{0.5}\frac{L}{b(h-a_0)^2} \tag{2}$$

$$f_{eq,3} = \frac{3}{2}\frac{D^f_{BZ,3}}{2.5}\frac{L}{b(h-a_0)^2} \tag{3}$$

where $f_{eq,2}$ and $f_{eq,3}$ are equivalent flexural strength strengths; $D^f_{BZ,2}$ and $D^f_{BZ,3}$ are the energy absorption capacities until deflections of δ_2 and δ_3 ($\delta_2 = \delta_L + 0.65$ mm and $\delta_3 = \delta_L + 2.65$ mm), excluding the triangular area up to the deflection of 0.3 mm; and δ_L is the deflection corresponding to the peak load up to 0.05 mm.

Table 7 lists the calculated parameters. By increasing the fiber aspect ratio and volume fraction, both the energy absorption capacities and the equivalent strengths were improved. The highest value of $f_{eq,2}$ was obtained for specimen S65-0.75, whereas the highest value of $f_{eq,3}$ was obtained for specimen S80-0.5. This indicates that using a higher amount of fibers is effective in improving flexural performance under small deflections, whereas using longer fibers is efficient in improving flexural performance under large deflections.

The following equations were used to obtain tensile stress versus strain laws; the material modeling is schematically illustrated in Fig. 10.

$$\sigma_1 = 0.7f_{MOR}(1.6-d),\ \sigma_2 = 0.45f_{eq,2}k_h,\ \sigma_3 = 0.37f_{eq,3}k_h \tag{4}$$

$$\varepsilon_1 = \sigma_1/E_c,\ \varepsilon_2 = \varepsilon_1 + 0.0001,\ \varepsilon_3 = 0.025 \tag{5}$$

Table 7 Parameters for modeling tensile stress block of SFR-HSC.

Name	$D^f_{BZ,2}$ (kNmm)	$D^f_{BZ,3}$ (kNmm)	$F_{eq,2}$ (MPa)	$F_{eq,3}$ (MPa)	σ_1 (MPa)	σ_2 (MPa)	σ_3 (MPa)	ε_1 (mm/mm)	ε_2 (mm/mm)	ε_3 (mm/mm)
S65-0.5	7.7	37.1	4.93	4.75	6.92	2.22	1.76	0.00021	0.00031	0.025
S80-0.5	10.7	56.3	6.85	7.21	7.80	3.08	2.79	0.00024	0.00034	0.025
S65-0.75	14.3	55.1	9.15	7.05	8.20	4.12	2.61	0.00025	0.00035	0.025

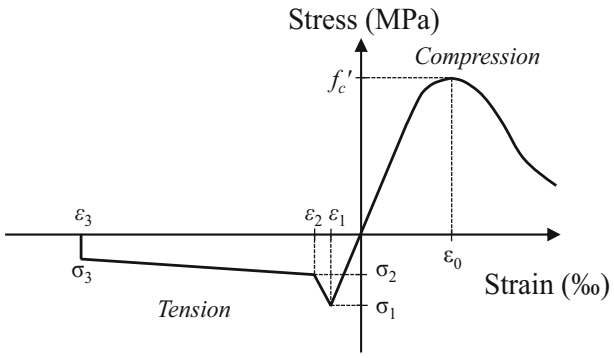

Fig. 10 Material modeling.

$$k_h = 1.0 - 0.6\frac{h - 12.5}{47.5} \quad |12.5 \le h \le 60|, \text{ [unit of h: cm]} \tag{6}$$

Here, f_{MOR} is the flexural strength, d is the effective beam depth, and E_c is the elastic modulus of concrete.

The calculated TSS models are shown in Fig. 11, and the parameters are summarized in Table 7. Specimen S65-0.75 exhibited the highest tensile strength of 8.2 MPa, whereas the highest residual tensile strength, σ_3, was obtained in specimen S80-0.5 as 2.8 MPa. This is consistent with the findings from flexural tests discussed above.

Complete material models under compression and tension for the SFR-HSC used in the current study were obtained by using Lee's compressive model (Lee et al. 2015) in Eq. (1) and the tensile models, suggested by RILEM TC 162-TDF, with suggested parameters from Table 7. Thus, these models can be adopted for sectional analysis of structural elements made of SFR-HSC.

3.2.4 Fracture Energy

In order to compare the fracture energy behaviors of SFR-HSCs according to the crack opening displacement (COD), the post-cracking tensile stress versus strain curves in Fig. 11 were transferred to the post-cracking tensile stress versus COD. For this, the following equation was adopted from AFGC recommendations (AFGC 2013): $f_{t,el}/E_c + w/l_c$, where $f_{t,el}$ is the cracking tensile strength, E_c is the elastic modulus, w is the COD, and l_c is the

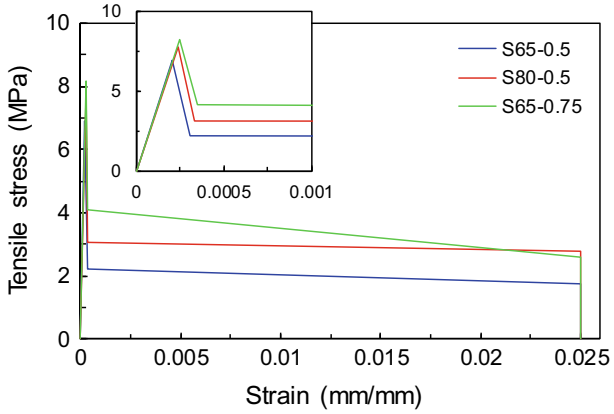

Fig. 11 Tensile stress versus strain models.

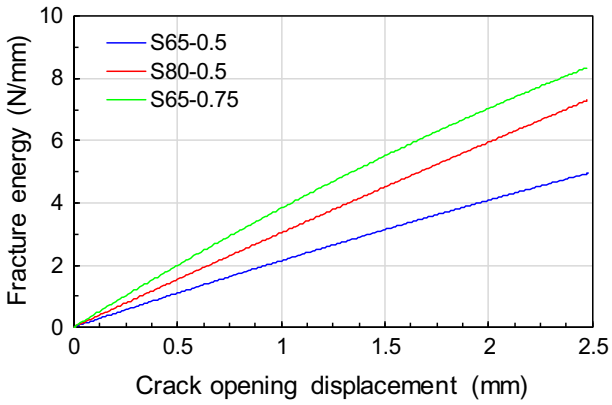

Fig. 12 Fracture energy versus COD curves.

characteristic length (=2/3 × beam height for rectangular beam). The cumulative fracture energies with COD are summarized in Fig. 12. It was obvious that the hooked steel fiber with a higher aspect ratio of 80 exhibited higher fracture energy capacity than that with a lower aspect ratio of 65, although the identical fiber volume fraction of 0.5% was adopted. In addition, the use of higher amount of hooked steel fibers resulted in an increase in the fracture energy capacity at the identical aspect ratio of 65. Consequently, the increases of fiber aspect ratio or amount are able to improve the fracture energy capacities.

4. Conclusions

Herein, the effects of W/B ratio and BFS replacement ratio upon concrete compressive strength were investigated to determine an optimized mixture. Based on the optimized mixture, the implications of using hooked steel fibers of various aspect ratios and volume fractions upon the mechanical properties of HSC were then evaluated. Lastly, to design structures made of SFR-HSC, complete material models of SFR-HSC under compression and tension were proposed. We made the following conclusions:

1. Concrete mixtures with a lower W/B ratio and higher replacement ratios of BFS up to 60% exhibited higher compressive strength than their counterparts. The optimum BFS replacement ratio varied between 50 and 60% in terms of the compressive strength developed in steam-cured HSC both early and during long-term aging.
2. The addition of hooked steel fibers slightly increased the compressive strength and increased the post-peak ductility significantly. In addition, the use of hooked steel fibers with smaller aspect ratios resulted in better HSC compressive behavior. The overall compressive stress–strain curve was predicted well by Lee's model.
3. HSC beams having V_f of 0.5% or more exhibited deflection-hardening behavior. The use of hooked steel fibers with the highest aspect ratio tested of 80 was more effective in improving the flexural strength, deflection capacity, energy absorption capacity, and residual

strength affecting shear resistance, relative to the use of hooked steel fibers with a smaller aspect ratio of 65. In particular, increasing the aspect ratio from 65 to 80 allowed a 0.25% volume reduction of the steel fiber content without any noticeable deterioration of energy absorption capacity. Finally, we proposed TSS models with appropriate parameters for all SFR-HSCs tested, based on the RILEM TC 162-TDF recommendations.

4. Fracture energy capacity of SFR-HSC was improved by increasing the aspect ratio or the amount of hooked steel fibers.

Acknowledgements

This work was supported by the Industrial Strategic Technology Development Program (10063488, Development of Earthquake Resisting Reinforced Concrete using Grade 700 MPa Reinforcing Bars for Enhancement of Seismic Safety) funded By the Ministry of Trade, Industry & Energy (MI, Korea).

Open Access

References

ACI Committee 318. (2014). *Building code requirements for structural concrete and commentary.* ACI 318-14 and ACI 318R-14, American Concrete Institute, Farmington Hills, Mich., USA, p 519.

AFGC. (2013). *Ultra high performance fibre-reinforced concretes. Interim recommendations* (p. 358). France: AFGC publication.

ASTM C1609/C1609 M. (2012). Standard test method for flexural performance of fiber-reinforced concrete (using beam with third-point loading), ASTM International, West Conshohocken, PA, pp. 1–9.

ASTM C 39/39 M. (2014). Standard test method for compressive strength of cylindrical concrete specimens, ASTM International, West Conshohocken, PA, pp. 1–7.

Banthia, N., & Nandakumar, N. (2006). Crack growth resistance of hybrid fiber reinforced cement composites. *Cement and Concrete Composites, 25*(1), 3–9.

Barnett, S. J., Soutsos, M. N., Millard, S. G., & Bungey, J. H. (2006). Strength development of mortars containing ground granulated blast-furnace slag: Effect of curing temperature and determination of apparent activation energies. *Cement and Concrete Research, 36*(3), 434–440.

Barros, J. A., Cunha, V. M., Ribeiro, A. F., & Antunes, J. A. B. (2005). Post-cracking behaviour of steel fibre reinforced concrete. *Materials and Structures, 38*(1), 47–56.

Bilodeau, A., & Malhotra, V. M. (2000). High-volume fly ash system: Concrete solution for sustainable development. *ACI Materials Journal, 97*(1), 41–48.

Bindiganavile, V., & Banthia, N. (2001). Polymer and steel fiber-reinforced cementitious composites under impact loading–Part 2: Flexural toughness. *ACI Materials Journal, 98*(1), 17–24.

Ezeldin, A. S., & Balaguru, P. N. (1992). Normal-and high-strength fiber-reinforced concrete under compression. *Journal of Materials in Civil Engineering, 4*(4), 415–429.

Jeon, J. K., Moon, H. Y., Ann, K. Y., Kim, H. S., & Kim, Y. B. (2006). Effect of ground granulated blast furnace slag, pulverized fuel ash, silica fume on sulfuric acid corrosion resistance of cement matrix. *International Journal of Concrete Structures and Materials, 18*(2E), 97–102.

Kinoshita, H., Circhirillo, C., SanMartin, I., Utton, C. A., Borges, P. H. R., Lynsdale, C. J., et al. (2014). Carbonation of composite cements with high mineral admixture content used for radioactive waste encapsulation. *Minerals Engineering, 59,* 107–114.

Kwon, K. Y., Yoo, D. Y., Han, S. C., & Yoon, Y. S. (2015). Strengthening effects of sprayed fiber reinforced polymers on concrete. *Polymer Composites, 36*(4), 722–730.

Lee, S. C., Oh, J. H., & Cho, J. Y. (2015). Compressive behavior of fiber-reinforced concrete with end-hooked steel fibers. *Materials, 8*(4), 1442–1458.

Mahmoud, E., Ibrahim, A., El-Chabib, H., & Patibandla, V. C. (2013). Self-consolidating concrete incorporating high volume of fly ash, slag, and recycled asphalt pavement. *International Journal of Concrete Structures and Materials, 7*(2), 155–163.

Menéndez, G. V. B. B., Bonavetti, V., & Irassar, E. F. (2003). Strength development of ternary blended cement with limestone filler and blast-furnace slag. *Cement and Concrete Composites, 25*(1), 61–67.

Mindess, S., Young, J. F., & Darwin, D. (2003). *Concrete* (p. 644). Upper Saddle River, NJ: Prentice Hall.

Myers, D., Kang, T. H., & Ramseyer, C. (2008). Early-age properties of polymer fiber-reinforced concrete. *International Journal of Concrete Structures and Materials, 2*(1), 9–14.

Parra-Montesinos, G. J. (2006). Shear strength of beams with deformed steel fibers. *Concrete International, 28*(11), 57–66.

RILEM TC162-TDF. (2000). Test and design methods for steel fibre reinforced concrete: Bending test. Materials and Structures, 33, 75–81

Roychand, R., De Silva, S., Law, D., & Setunge, S. (2016). Micro and nano engineered high volume ultrafine fly ash cement composite with and without additives. *International Journal of Concrete Structures and Materials, 10*(1), 113–124.

Soroushian, P., & Bayasi, Z. (1991). Fiber type effects on the performance of steel fiber reinforced concrete. *ACI Materials Journal, 88*(2), 129–134.

Weibull, W. (1939). A statistical theory of the strength of materials. *Proceedings, The Royal Swedish Institute for Engineering Research*, 151 (pp. 1–45).

Wille, K., & Parra-Montesinos, G. J. (2012). Effect of beam size, casting method, and support conditions on flexural behavior of ultra-high-performance fiber-reinforced concrete. *ACI Materials Journal, 109*(3), 379–388.

Yao, W., Li, J., & Wu, K. (2003). Mechanical properties of hybrid fiber-reinforced concrete at low fiber volume fraction. *Cement and Concrete Research, 33*(1), 27–30.

Yazıcı, Ş., İnan, G., & Tabak, V. (2007). Effect of aspect ratio and volume fraction of steel fiber on the mechanical properties of SFRC. *Construction and Building Materials, 21*(6), 1250–1253.

Yoo, D. Y., Banthia, N., Yang, J. M., & Yoon, Y. S. (2016a). Size effect in normal- and high-strength amorphous metallic and steel fiber reinforced concrete beams. *Construction and Building Materials, 121,* 676–685.

Yoo, D. Y., Banthia, N., & Yoon, Y. S. (2016b). Flexural behavior of ultra-high-performance fiber-reinforced concrete beams reinforced with GFRP and steel rebars. *Engineering Structures, 111,* 246–262.

Yoo, D. Y., Kang, S. T., & Yoon, Y. S. (2016c). Enhancing the flexural performance of ultra-high-performance concrete using long steel fibers. *Composite Structures, 147,* 220–230.

Yoo, D. Y., & Yoon, Y. S. (2015). Structural performance of ultra-high-performance concrete beams with different steel fibers. *Engineering Structures, 102,* 409–423.

Yoo, D. Y., & Yoon, Y. S. (2016). A review on structural behavior, design, and application of ultra-high-performance fiber-reinforced concrete. *International Journal of Concrete Structures and Materials, 10*(2), 125–142.

Yoo, D. Y., Yoon, Y. S., & Banthia, N. (2015). Flexural response of steel-fiber-reinforced concrete beams: Effects of strength, fiber content, and strain-rate. *Cement and Concrete Composites, 64,* 84–92.